The implications of temporal variability in wave-particle interactions in Earth's Radiation Belts

C. E. J. Watt[1,2], H. J. Allison[3], R. L. Thompson[4], S. N. Bentley[1,2], N. P. Meredith[5], S. A. Glauert[5], R. B. Horne[5], I. J. Rae[6,2]

[1]Department of Meteorology, University of Reading, Reading, UK
[2]Department of Mathematics, Physics and Elecrical Engineering, Northumbria University, Newcastle upon Tyne, UK
[3]GFZ, German Centre for Geosciences, Potsdam, Germany
[4]Department of Mathematics and Statistics, University of Reading, Reading, UK
[5]British Antarctic Survey, Cambridge, UK
[6]Mullard Space Science Laboratory, University College London, London, UK

Key Points:

- Plasmaspheric hiss wave-particle interactions are observed to exhibit large variability over timescales ranging from 2 minutes to 9 hours
- Numerical diffusion experiments are sensitive to variability timescales, even when experiments experience the same time-integrated diffusion
- Experiments reveal more diffusion from average of all diffusion coefficients than when coefficient is constructed from averaged inputs

Corresponding author: C. E. J. Watt, clare.watt@northumbria.ac.uk

This article has been accepted for publication and undergone full peer review but has not been through the copyediting, typesetting, pagination and proofreading process, which may lead to differences between this version and the Version of Record. Please cite this article as doi: 10.1029/2020GL089962.

Abstract

Changes in electron flux in Earth's outer radiation belt can be modeled using a diffusion-based framework. Diffusion coefficients D for such models are often constructed from statistical averages of observed inputs. Here we use stochastic parameterization to investigate the consequences of temporal variability in D. Variability timescales are constrained using Van Allen Probe observations. Results from stochastic parameterization experiments are compared with experiments using D constructed from averaged inputs, and an average of observation-specific D. We find that the evolution and final state of the numerical experiment depends upon the variability timescale of D; experiments with longer variability timescales differ from those with shorter timescales, even when the time-integrated diffusion is the same. Short variability timescale experiments converge with solutions obtained using an averaged observation-specific D, and both exhibit greater diffusion than experiments using the averaged-input D. These experiments reveal the importance of temporal variability in radiation belt diffusion.

Plain Language Summary

Electron behavior in the Earth's radiation belts can only be modeled successfully if we average important processes over a long time. The direction of the high-energy electron motion, or its energy, can be changed through interaction with an electromagnetic wave, but these interactions are energy-dependent. The efficacy of the interaction depends upon the strength of the electromagnetic waves, but also on the local density of the plasma and the magnetic field strength. In many models, years of spacecraft measurements are averaged to provide input into the models. We have shown in previous work that the variability of the wave-particle interactions is much larger than that suggested by averaged models. Here, we show the implications of this variability when applied within a radiation belt model. We use a technique that is popular in numerical weather prediction and climate modelling to capture the natural variability of the wave-particle interaction. We demonstrate that the results from the model depend sensitively on the presence, and timescale, of the variability. Some of the variability may be captured by constructing our averages in a different way, but our efforts first require better descriptions of how wave-particle interactions vary, and on what timescales.

1 Introduction

Physics-based radiation belt models of electron behaviour often focus on the wave-particle interactions that accelerate and scatter particles or contribute to radial diffusion. These models make considerable use of quasilinear theory to describe the wave-particle interactions (e.g. Lyons et al. (1972); Ripoll et al. (2020)) and can be used to study the flux of high-energy electrons on a range of timescales, from single storms (e.g. Ripoll et al., 2016; Allison et al., 2019; Li et al., 2016; Drozdov et al., 2015) to multiple solar cycles (Glauert et al., 2018). The strength of quasilinear theory is that it can be used to describe wave-particle interactions, whose characteristic timescales are much less than a second, in models whose timescales are considerably longer.

The quasilinear theory of wave-particle interactions describes the slow (relative to the wave period) evolution of the particle distribution function, f, due to resonant interactions. Diffusion coefficients describe the efficacy of this process, combining information regarding the intensity of the waves as a function of frequency and wave-normal angle, and the resonant condition between the electrons and the waves. In a Fokker-Planck model, the diffusion coefficients contain all the important sub-grid physics, hence our choice of methods to model the diffusion coefficients becomes a key part of the model.

Models of diffusion coefficients largely employ two different strategies: parameterized "average" models and event-specific types. Parameterized models offer comprehen-

sive spatial coverage, and are often parameterized by a geomagnetic activity index. For example, the energy and pitch-angle diffusion due to whistler mode hiss or chorus has been parameterized by Kp (e.g. Spasojevic et al. (2015); Wang et al. (2019)) or AE (e.g. Horne et al. (2013); Meredith et al. (2018, 2020))

The availability of new datasets (e.g. from the NASA Van Allen Probes and the JAXA Arase mission) have encouraged the construction of "event-specific" models of diffusion coefficients. For example, event-specific models of whistler-mode waves can include not only the variation of wave characteristics, but the variation of the magnetic field and number density that controls the resonant condition between waves and electrons (e.g. Tu et al., 2014; Ripoll et al., 2016, 2017, 2019; Zhao et al., 2018) or indeed the wave amplitudes themselves (e.g. Malaspina et al., 2016, 2018). Event-specific models capture more of the variability in wave-particle interactions (see e.g. Ripoll et al. (2017)), and perhaps importantly, more of the extremes in this process than averaged parameterized models. In what follows, we investigate the effects of including temporal variability in a more general diffusion model, where we build a stochastic parameterization (Berner et al., 2017) from a statistical database of observations. We focus on pitch-angle diffusion due to plasmapheric hiss (e.g. Meredith et al. (2018); Hartley et al. (2018); Malaspina et al. (2017); Li et al. (2015)).

2 Methods

2.1 Constructing $D_{\alpha\alpha}(t)$

In Figure 1, we show the probability distribution function of observation-specific bounce-averaged pitch-angle diffusion coefficients $D_{\alpha\alpha}(X_i, Y_i)$ constructed using 4 years of observations from Van Allen Probe A. Individual pairs of observations X_i, Y_i of ratio of plasma frequency to electron gyrofrequency ($X_i = \omega_{pe}/\Omega_e$) and wave intensity at $f = 252$ Hz ($Y_i = \delta B^2$) are used as input to the calculation of each $D_{\alpha\alpha}(\alpha)$. Diffusion coefficients are shown for $E = 0.5$ MeV. Full details of other inputs and method of calculation are described in (Watt et al., 2019).

Figure 1(a) demonstrates a large amount of variability in $D_{\alpha\alpha}(\alpha)$. Where the diffusion coefficient is weakest ($60^\circ \lesssim \alpha \lesssim 75^\circ$), the variability is highest. There is a region at $\alpha \sim 75^\circ$ where the resonant condition is not satisfied, and so there is no diffusion across this pitch-angle range. The diffusion coefficient is rarely greater than 10^{-5} s^{-1} (similar to a diffusion timescale of 1 day) across all pitch-angles.

It is possible to construct an estimate of the average diffusion in two ways Shprits et al. (2009); Horne et al. (2013); Wang et al. (2019); Zhu et al. (2019)) : (i) using the average values of input conditions $D_{\alpha\alpha}(\langle X_i\rangle, \langle Y_i\rangle)$ where $\langle \ldots \rangle$ indicates an arithmetic mean (c.f. methods of Shprits et al. (2009); Horne et al. (2013); Wang et al. (2019); Zhu et al. (2019)) or (ii) constructing an average of each observation specific diffusion coefficient $\langle D_{\alpha\alpha}(X_i, Y_i)\rangle$. In Figure 1(a), the white solid line indicates the value of $\langle D_{\alpha\alpha}(X_i, Y_i)\rangle$, and the dashed line indicates $D_{\alpha\alpha}(\langle X_i\rangle, \langle Y_i\rangle)$. At all pitch-angles $\langle D_{\alpha\alpha}(X_i, Y_i)\rangle > D_{\alpha\alpha}(\langle X_i\rangle, \langle Y_i\rangle)$ and for $\alpha < 60^\circ$, $\langle D_{\alpha\alpha}(X_i, Y_i)\rangle \sim 2D_{\alpha\alpha}(\langle X_i\rangle, \langle Y_i\rangle)$. $\langle D_{\alpha\alpha}(X_i, Y_i)\rangle$ is positive over a slightly larger range of α than $D_{\alpha\alpha}(\langle X_i\rangle, \langle Y_i\rangle)$. .

Two example probability density functions for $\alpha = 30^\circ$ and $\alpha = 60^\circ$ are shown in Figure 1(b) on a logarithmic scale, indicating the non-Gaussian nature of the distributions. Figure 1(c) shows the quantile-quantile plot for the probability distribution function of $D_{\alpha\alpha}(\alpha = 45^\circ)$, representative of all the probability distribution functions shown in Figure 1(a). The deviations from standard normal quantiles (red line) towards the right-hand side of the plot indicate the presence of a statistically heavy tail.

We construct a variable $D_{\alpha\alpha}(t)$ that preserves the underlying distribution and range of $D_{\alpha\alpha}$ as displayed in Figure 1. We choose a simple method where the function $D_{\alpha\alpha}(\alpha)$

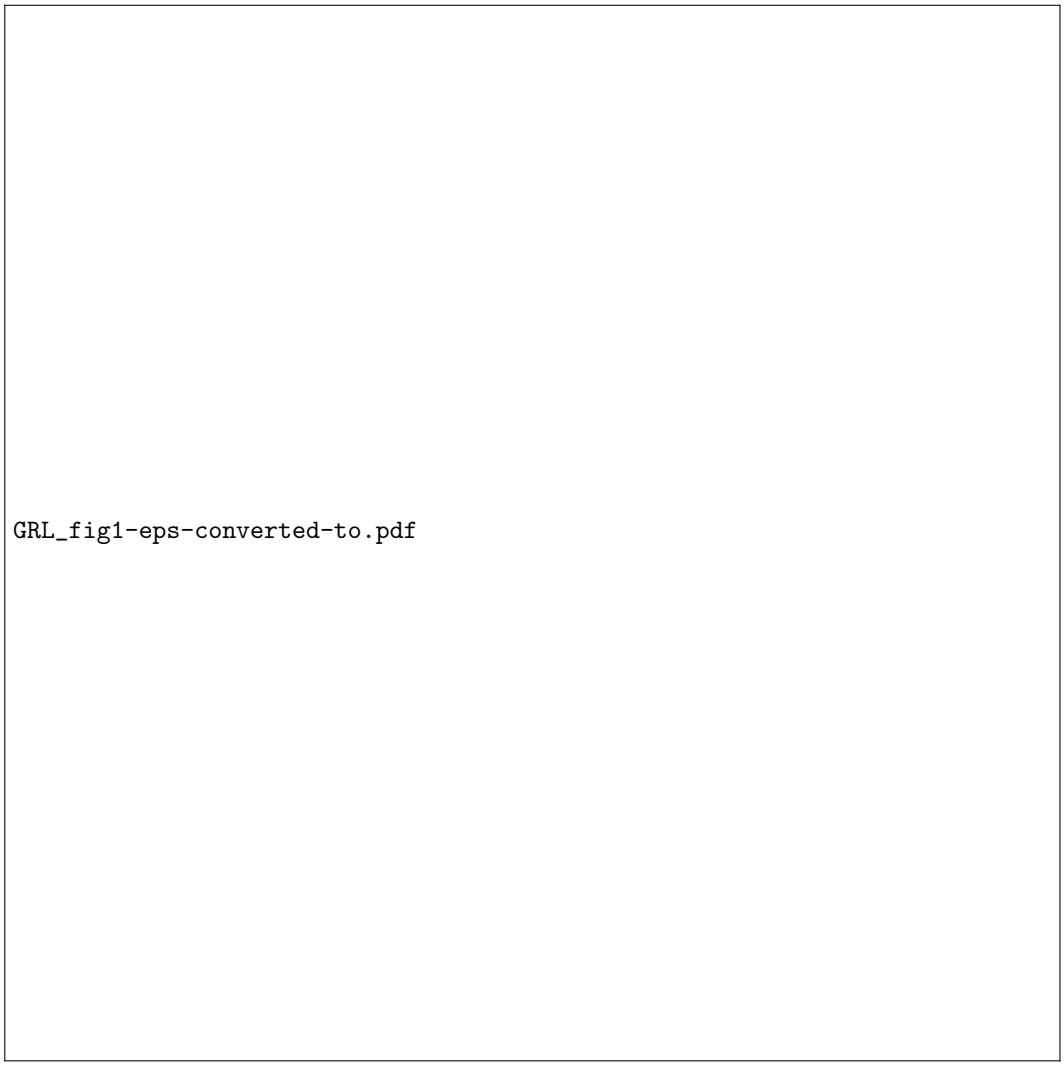

Figure 1. (a) Distribution of 2377 diffusion coefficients calculated using Pitch Angle Diffusion for Ions and Electrons (PADIE - Glauert and Horne (2005)) algorithm for co-located simultaneous observations of wave intensity, number density and magnetic field strength over a four-year interval. Observations are limited to a small range of magnetic local time (09 − 10 MLT), magnetic latitude ($-5^\circ \leq \lambda \leq +5^\circ$ and L^* ($2.95 \leq L^* \leq 3.05$). Each column of the shaded region is a normalised probability distribution function estimated with a kernel density method. The solid white line indicates the average of the distribution of diffusion coefficients, and the dashed white line indicates a diffusion coefficient calculated from the averaged input values of wave intensity, number density and magnetic field strength over the same four-year interval. (b) Estimated probability distribution function when $\alpha = 30^\circ$ (dark blue) and $\alpha = 60^\circ$ (orange). (c) Quantile-quantile plot for the probability distribution function for $\alpha = 45^\circ$. Blue '+' indicate the quantiles of the distribution of $D_{\alpha\alpha}(\alpha = 45^\circ)$, and the red line indicates the expected behaviour of the quantiles if the probability distribution function were normal.

is randomly selected from the 2377 calculated values and kept constant for a period $t = \Delta t$ (note the importance of retaining the functional dependence of $D_{\alpha\alpha}$ on the pitch-angle). At the end of this period, another $D_{\alpha\alpha}(\alpha)$ is chosen and kept constant for the same time period. The modelled time-series is denoted $D_{rand}(\Delta t)$, and our choices of Δt are motivated in the following section.

2.2 Timescales

To construct $D_{rand}(\Delta t)$, an estimate of the temporal scales of variability of $D_{\alpha\alpha}$ is required. Since orbiting spacecraft that sample the outer radiation belt (e.g. NASA Van Allen probes, JAXA Arase, CRRES) traverse this region relatively quickly, distinguishing spatial and temporal variations is difficult. We obtain estimates for the temporal scale of variability by studying the temporal evolution of inputs to the diffusion coefficients (magnetic field strength B_0, number density n_e and wave intensity δB^2 at $f = 252$ Hz), and the diffusion coefficients themselves, calculated in our previous work (Watt et al., 2019).

Figure 2 shows a month of variations from 3 Nov 2012 to 3 Dec 2012 observed in the $L^* = 3.0$ bin. In each panel, circles indicate mean values and errorbars indicate standard deviations of both observations and our calculated $D_{\alpha\alpha}(E = 0.5 \text{ MeV}, \alpha = 30^\circ)$ during each pass of Van Allen Probe A through the bin. It takes around 2 minutes for the spacecraft to traverse the bin, and around 9 hours to return to a similar spot. Note that since location bins are very small in L^*, MLT and magnetic latitude λ, the spacecraft is not guaranteed to traverse the same bin each orbit; it can be more than 9 hours from one data point shown in Figure 2 to the next.

Panel (a) shows the variability of the ambient magnetic field B_0. The standard deviation of the magnetic field is due to the spatial variation of B_0 as the spacecraft traverses the radial distance $2.95 < L^* < 3.05$. The variation between passes is very small compared to the variation during a pass, with the exception of the pass on the 18 November 2012 . For n_e (panel (b)), the variation from one pass to the next is much greater than the variation seen within each pass. There is a moderate geomagnetic storm with minimum Dst reaching ~ 110 nT that commences near midnight on 13 November 2012 (see gray trace in Figure 2(b)). Prior to this time, n_e mainly lies between 1.5-2$\times 10^9$ m^{-3}, but after the storm starts, n_e is depressed to between 0.5-1.5$\times 10^9$ m^{-3}, and remains so at least until the end of the month. The variations in wave intensity δB^2 are demonstrated in panel 2(c). The wave intensity is significantly more variable than B_0 or n_e, varying over at least three orders of magnitude over the interval presented (cf. Figure 5 in Ripoll et al. (2017)). Interestingly, the variation of hiss power during the storm appears opposite to that reported by Malaspina et al. (2018) (i.e. that plasmaspheric hiss power decreases with decreasing density) although storms may prove to display different wave power dependencies than in quiet times. The variation in δB^2 between spacecraft traverses through the bin is usually much bigger than the variation seen during each pass.

Figure 2(d) shows the variability in the calculated $D_{\alpha\alpha}(E = 0.5 \text{ MeV}, \alpha = 30^\circ)$ during November 2012 (calculations of mean and standard deviation are for $\log_{10}(D_{\alpha\alpha})$). The variability of $D_{\alpha\alpha}$ during each pass should be interpreted as an estimate of the uncertainty in its calculation. The variation in diffusion coefficient largely tracks the variation in the wave intensity, although the increase in diffusion is much more pronounced in the middle of the month than the increase in wave intensity. This is due to the systematic decrease in electron number density in this bin as a result of the storm as pitch-angle diffusion increases when the density decreases when all other parameters are kept constant (e.g. Glauert and Horne (2005)).

We conclude from Figure 2(d) that temporal scales of variability of $D_{\alpha\alpha}$ in this observation bin lie between 2 minutes and 9 hours . We therefore choose two temporal scales $\Delta t = 2$ minutes and $\Delta t = 6$ hours for our study to span this range. We stress that

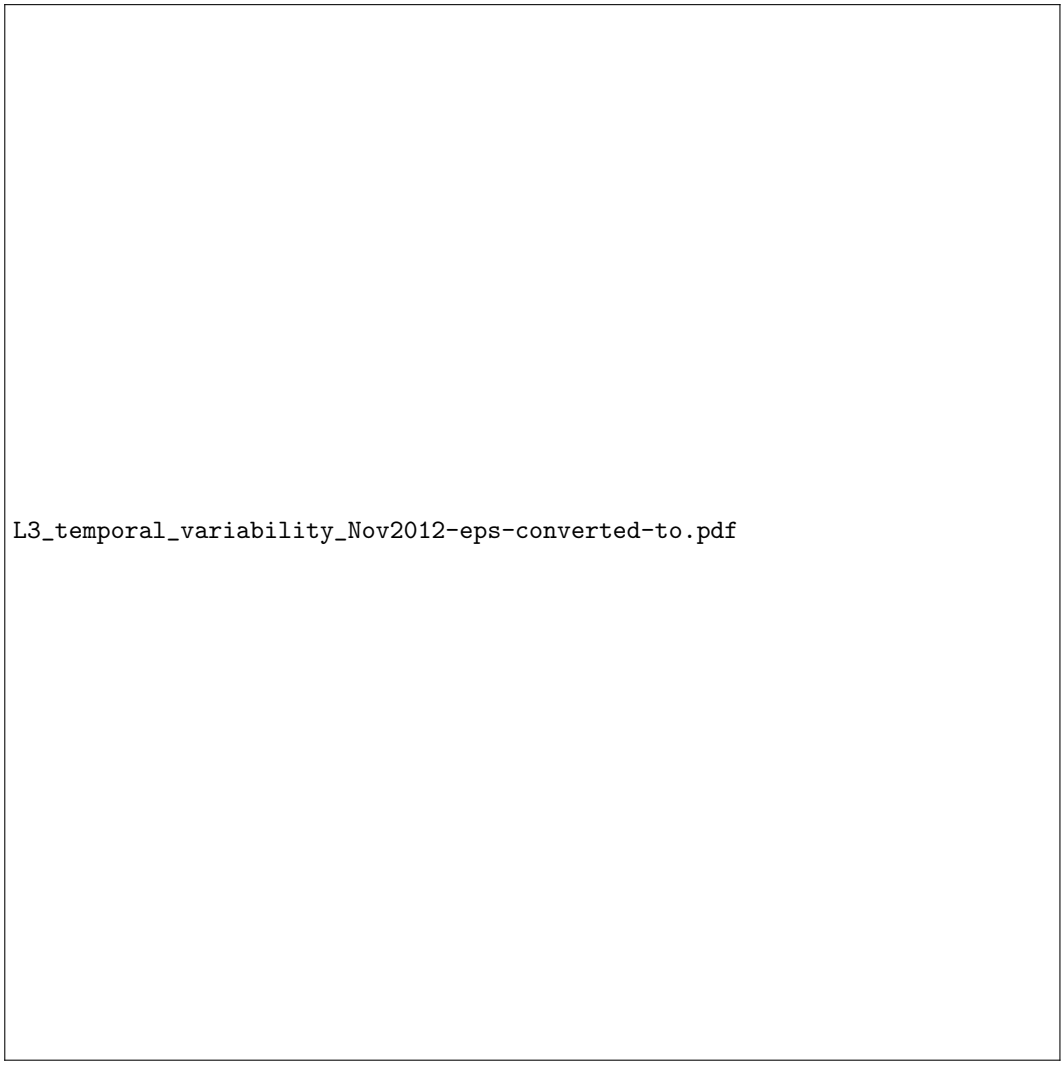

Figure 2. Figure demonstrating temporal variability of inputs to diffusion coefficient, and coefficient itself, during the month of November 2012 as Van Allen Probe A passed through the $L^* = 3.0$ bin (see text for details of bin dimensions). (a) Shows magnetic field variations, (b) number density variations, (c) wave intensity variations and (d) the resulting variability in the calculated diffusion coefficient for $E = 0.5$ MeV and $\alpha = 30°$. Circles indicate the mean of the observations made during a single pass through the bin, and errorbars indicate the standard deviation. In panels (c) and (d), mean and standard deviations were calculated for the logarithm of the displayed quantity. In panel (b), the Dst value over the same period is indicated in gray.

these choices serve an illustrative purpose in the following numerical experiments and reflect the constraints provided by spacecraft coverage (c.f. Ripoll et al. (2017)). We wish to investigate *whether* pitch-angle diffusion depends on Δt; a full characterisation of the dependence of diffusive processes on the full range of possible Δt is a larger task left for future work.

2.3 Numerical diffusion experiments

For the illustration presented here, we assume that pitch-angle diffusion dominates, and ignore energy diffusion due to plasmaspheric hiss. One-dimensional diffusion experiments at a single energy are performed with different choices of bounce-averaged diffusion coefficients $D_{\alpha\alpha}(t)$. The energy $E = 0.5$ MeV is chosen because the original calculations of the distribution of $D_{\alpha\alpha}$ were performed at this energy. Results may also vary with energy, which will be a focus of future work.

The time evolution of the phase space density at each pitch angle, f, can be found by solving the 1-D Fokker Planck equation for pitch angle diffusion, given by

$$\frac{\partial f}{\partial t} = \frac{1}{T \sin 2\alpha} \left(\frac{\partial}{\partial \alpha} \left(D_{\alpha\alpha}(t) T \sin 2\alpha \frac{\partial f}{\partial \alpha} \right) \right) - \frac{f}{\tau_L} \tag{1}$$

where T(α) is given by

$$T(\alpha) = 1.3802 - 0.3198(\sin \alpha + \sin^{1/2} \alpha). \tag{2}$$

The second term on the right hand side of equation (1) accounts for losses due to atmospheric collisions and the loss timescale τ_L is taken to be a quarter of the bounce period inside the loss cone and infinite outside (Shprits et al., 2008).

In the following analysis, equation (1) is solved using an explicit time stepping scheme in steps of 0.1 s. The pitch angle grid has a resolution of 1° and boundary conditions at $\alpha = 0°$ and $\alpha = 90°$ are required to define the calculation domain. We assume that far into the loss cone, collisions are sufficient for the phase space density distribution to be isotropic, and use $\frac{\partial f}{\partial \alpha} = 0$ at 0° and 90° (see e.g. Glauert et al. (2014)). All of the following experiments initialise the simulation with an isotropic pitch angle distribution, assuming an electron flux of 5×10^3 cm^{-2}s^{-1}sr^{-1}keV^{-1} for all pitch angles; this distribution is then allowed to evolve over a 30 day period.

We run a series of numerical experiments using the diffusion coefficients displayed in Figure 1. Specifically, each numerical experiment employs the same initial and boundary conditions, and they differ through the choice of $D_{\alpha\alpha}(t)$:

1. Ensemble experiments with $D_{\alpha\alpha}(t) = D_{rand}(\Delta t)$ with $\Delta t = 2$ minutes and 6 hours. The ensembles each contain 60 individual scenarios where a different random selection of $D_{\alpha\alpha}(\alpha)$ is drawn from the observed distribution (see Figure 1). [Ensemble convergence is demonstrated in the Supporting Information].
2. Constant diffusion experiment where $D_{\alpha\alpha}(t) = D_{\alpha\alpha}(\langle X_i \rangle, \langle Y_i \rangle) =$ constant (represented by dashed line in Figure 1(a)).
3. Constant diffusion experiment where $D_{\alpha\alpha}(t) = \langle D_{\alpha\alpha}(X_i, Y_i) \rangle =$ constant (represented by solid line in Figure 1(a)).

The number of unique diffusion coefficients in the distribution is 2377, defined in each case for $0 < \alpha < 90°$, and so given uniform sampling of the distribution, the $\Delta t =$ 2 minutes ensemble is likely to have sampled all coefficients after ~ 3.3 days. and the $\Delta t = 6$ hours ensemble after $\sim$ 400 days. Experiments are run to 30 days, with the caveat that the $\Delta t = 2$ minutes ensemble may show signs of oversampling of the discrete distribution. The experiments presented here do not distinguish between the amount

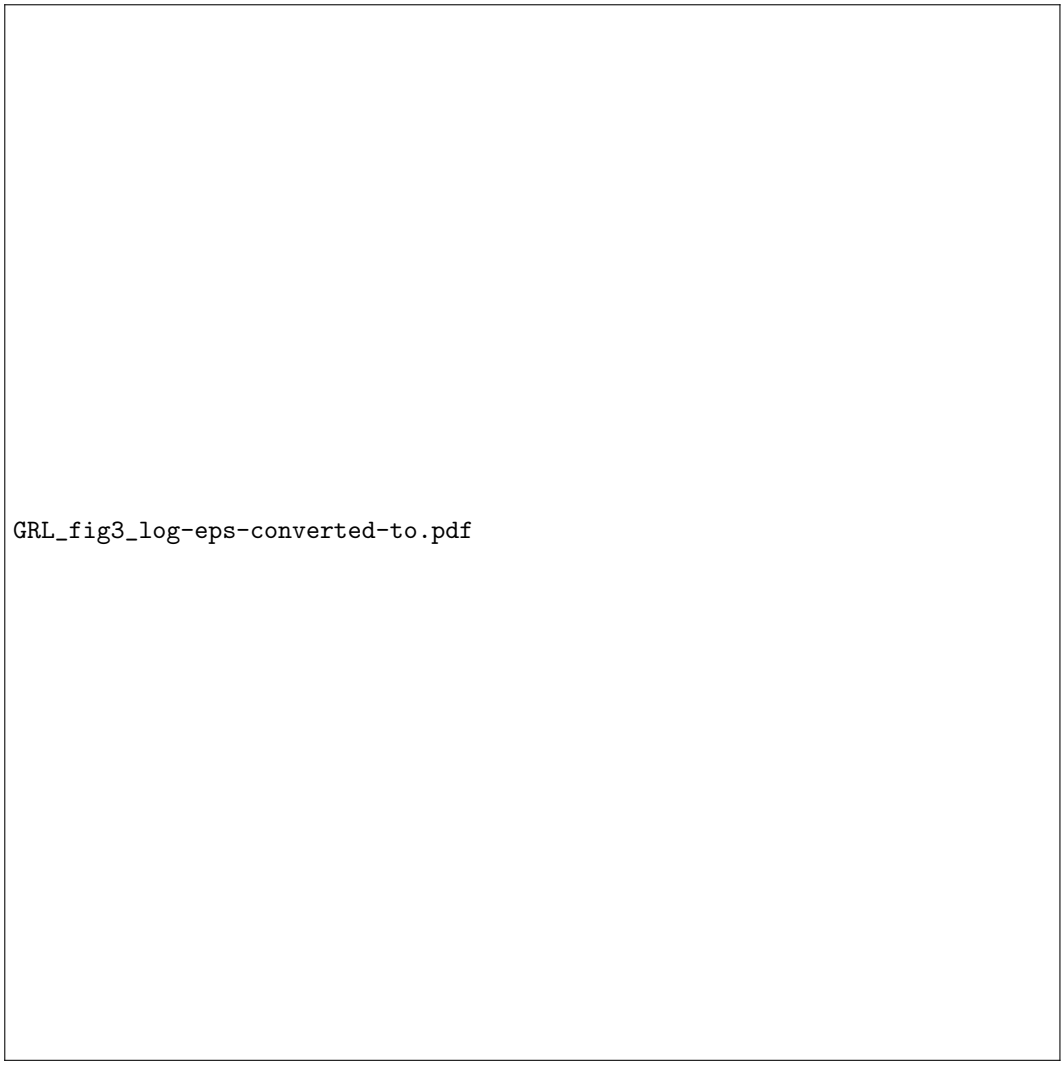

Figure 3. Examples of the distribution function solution from 1D diffusion experiments with (a) $D_{\alpha\alpha}(t) = D_{rand}(\Delta t = 6\text{h})$, (b) average diffusion coefficient $D_{\alpha\alpha} = \langle D_{\alpha\alpha}(X_i, Y_i)\rangle$ and (c) average diffusion coefficient $D_{\alpha\alpha} = D_{\alpha\alpha}(\langle X_i\rangle, \langle Y_i\rangle)$. An artifical floor has been applied to the data at $f = 10^0$ cm^{-1}s^{-1}sr^{-1}keV^{-1} since values of f are very small inside the loss cone.

or nature of temporal variability on different timescales, even though in reality variations on ~ 2 minute timescales are likely to have different causes than those on ~ 6 hour timescales. Our aim is to investigate the consequences of variability, and how the solutions to the diffusion equation depend on timescale with all other factors treated equally.

3 Results

In general, each member of the ensemble experiments evolves less smoothly compared to the case where a constant diffusion coefficient is used. An example is shown in Figure 3, where panel (a) displays the evolution of f during a single ensemble member from the numerical experiment where the diffusion coefficient is randomly varied $D_{\alpha\alpha}(t) = D_{rand}(\Delta t = 6\text{h})$, and panels (b) and (c) show the evolution of f during the averaged experiments with $D_{\alpha\alpha}(t) = \langle D_{\alpha\alpha}(X_i, Y_i)\rangle = \text{constant}$ and $D_{\alpha\alpha}(t) = D_{\alpha\alpha}(\langle X_i\rangle, \langle Y_i\rangle) =$

constant, respectively. Five days of evolution are shown. Given the initial and boundary conditions of the numerical experiments, and important features of the diffusion coefficients, it is expected that $f(\alpha)$ will rapidly approach zero as α tends to zero, and the values of $f(\alpha \lesssim 75°)$ will decrease as the diffusion progresses.

In the constant diffusion coefficient case, the variations in $f(\alpha)$ as a function of time are very smooth. There is more diffusion in panel (b) than in panel (c), reflecting that $\langle D_{\alpha\alpha}(X_i, Y_i)\rangle > D_{\alpha\alpha}(\langle X_i\rangle, \langle Y_i\rangle)$. The scenario where the diffusion coefficient is randomly varied often seems quite flat, with sporadic sudden changes in the evolution of f across all α, notably at $t \sim 1.7$, 2.5, 3.5 and 4.8 days. The sudden changes indicate times when a large $D_{\alpha\alpha}$ has been chosen from the distribution, and the solution after 30 days in each member of the ensemble is dependent upon the number of large jumps experienced. The times where the solution is practically constant (e.g. from $t \sim 3.6$ days to $t \sim 4.8$ days) indicate extended periods where mainly very small values of $D_{\alpha\alpha}(\alpha)$ have been chosen. There are also times where the value of f at a constant pitch-angle appears to experience brief increases with time (see e.g. $\alpha = 20°$ for $2.6 < t < 3.6$ days and for $20 < \alpha < 75$ at $t = 4.8$ days). These occur during times when $D_{\alpha\alpha}(\alpha)$ significantly changes shape from one Δt period to the next, and are most obvious in numerical experiments where $\Delta t = 6$ hours (i.e. the variation time is slow). During experiments with fast variations of $D_{\alpha\alpha}(\alpha)$, small increases in f are seen only for a very short time.

All solutions tend towards a picture similar to the top of Figure 3(a) where $f(\alpha > 75°)$ remains at the initial condition, and is elsewhere reduced to small values due to pitch-angle scattering and removal of phase space density in the loss cone. Snapshots of the process after 2, 10 and 30 days can be seen in Figure S1 of the supplementary information.

The temporal evolution and probability density functions of the ensemble experiments are shown in Figure 4 for a single value of α. In panel (a), the median of $f(\alpha = 30°)$ from the two ensemble experiments are indicated in orange ($\Delta t = 2$ minutes) and red ($\Delta t = 6$ hours). Results from the two constant $D_{\alpha\alpha}(\alpha)$ experiments are indicated in solid black ($D_{\alpha\alpha}(t) = \langle D_{\alpha\alpha}(X_i, Y_i)\rangle$) and dashed black ($D_{\alpha\alpha}(t) = D_{\alpha\alpha}(\langle X_i\rangle, \langle Y_i\rangle)$) lines, respectively. Panel (b) indicates the mean of the time-integrated diffusion coefficients from each set of ensemble experiments, demonstrating that by this measure, the two experiments experience very similar "total" diffusion. Panels (c) and (d) show column-normalised probability density estimates of each ensemble experiment for $\Delta t = 2$ minutes and 6 hours. From Figure 1, we can see that $\langle D_{\alpha\alpha}(X_i, Y_i)\rangle > D_{\alpha\alpha}(\langle X_i\rangle, \langle Y_i\rangle)$, so it is always expected that the black solid line will lie below the black dashed line in Figure 4(a). That is, the diffusion due to the average of all the diffusion coefficients is more than the diffusion due to the diffusion coefficient constructed from averaged inputs. The ratio of $f(\alpha = 30°)$ solutions of the two constant numerical experiments after 30 days is around 3.3.

The $\Delta t = 2$ minutes ensemble exhibits a time history very similar to the constant $D_{\alpha\alpha}(t) = \langle D_{\alpha\alpha}(X_i, Y_i)\rangle$ experiment, with very little spread in solutions. The median of the $\Delta t = 2$ minutes experiment tracks the $\langle D_{\alpha\alpha}(X_i, Y_i)\rangle$ experiment very well, until $t \sim 20$ days. At this point, the median of the ensemble indicates additional diffusion from the constant diffusion experiment and we can see from Figure 4(c) that the variability of the solutions increases. For a constant diffusion coefficient, the solution is likely to asymptotically approach a limit that takes into account the boundary conditions and is defined by the diffusion lifetime. However, when the shape and strength of the diffusion coefficient varies in time, there is no such limit and no associated lifetime, and diffusion is enhanced.

The time history of the $\Delta t = 6$ hours ensemble shows slightly slower diffusion initially in the median of the ensemble in Figure 4(a), and there is a large spread in the so-

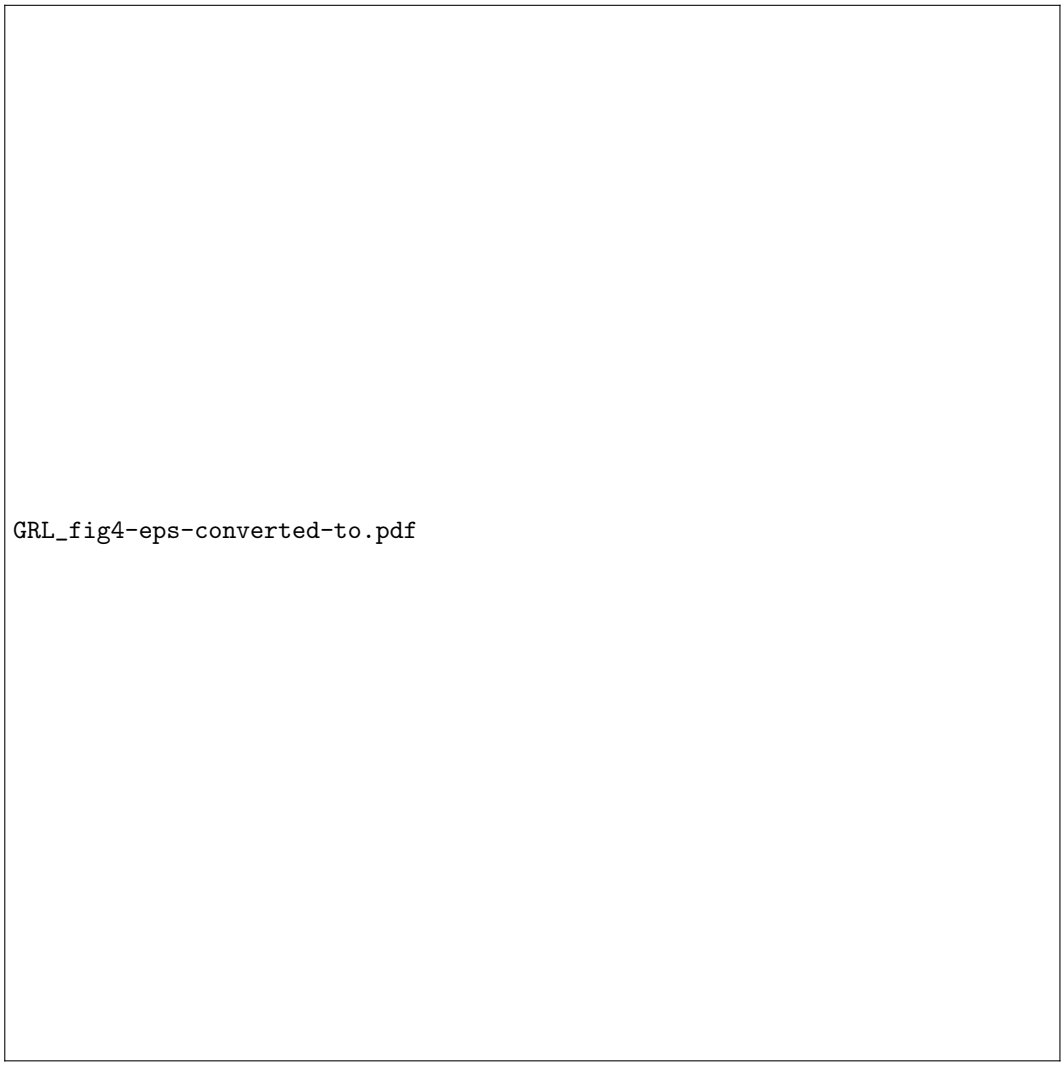

Figure 4. Evolution of $f(\alpha = 30^\circ)$ and time-averaged diffusion coefficients from ensemble experiments. (a) The solid black line indicates the evolution of the numerical experiment with constant $D_{\alpha\alpha}(t) = \langle D_{\alpha\alpha}(X_i, Y_i)\rangle$ and the dashed black line indicates the evolution of the numerical experiment with constant $D_{\alpha\alpha}(t) = D_{\alpha\alpha}(\langle X_i\rangle, \langle Y_i\rangle)$. Orange and red solid lines indicate the median of the ensemble numerical experiments for $\Delta t = 2$ minutes and $\Delta t = 6$ hours, respectively. (b) Mean time-integrated $D_{\alpha\alpha}$ for each ensemble experiment. (c) and (d) Column-normalised probability density functions of the ensemble numerical experiment for $\Delta t = 2$ minutes and $\Delta t = 6$ hours, respectively.

lutions (see Figure 4(d)). For $\Delta t = 6$ hours, the median $f(\alpha = 30°)$ decreases at a roughly constant rate until around 25 days and the final values of $f(\alpha = 30°)$ are on average much lower than in the other experiments.

4 Discussion

We have demonstrated that the evolution of the phase space density in an idealised diffusion experiment depends not only on *whether* the diffusion coefficient varies with time, but also on the *timescale* of that variation. There are three notable differences in the ensemble results for $\Delta t = 2$ minutes and $\Delta t = 6$ hours: differences in the evolution of median f, i.e. the trend in the behaviour of the ensemble, differences in the variance of the ensembles, and differences in the final values of f between the two ensembles. It is important to note that both the ensemble experiments, with $\Delta t = 2$ minutes and $\Delta t = 6$ hours, experience almost exactly the same time-integrated diffusion (see Figure 4(b)). Yet both the evolution of each ensemble, and the final state after 30 days, is markedly different and depends upon the timescale Δt. Most importantly, for $\Delta t = 6$ hours, most members of the ensemble experiment experience much more diffusion and reach lower values of $f(\alpha = 30°)$ than the two similar solutions (i.e. the ensemble result with $\Delta t = 2$ minutes, and the averaged result with $D_{\alpha\alpha}(t) = \langle D_{\alpha\alpha}(X_i, Y_i)\rangle$). We have begun investigations into why there are such differences in the two ensembles. We note that a key feature of our ensemble experiments is that the shape of the diffusion coefficient $D_{\alpha\alpha}(\alpha)$ changes with time, in addition to the strength of the diffusion coefficient and remind the reader that with a temporally-varying $D_{\alpha\alpha}(\alpha)$, there is no longer a well-defined lifetime.

It is important to note that the averaged $\langle D_{\alpha\alpha}(X_i, Y_i)\rangle$ result is a good approximation of the ensemble median when timescales of variation are short. The diffusion coefficient constructed from averaged inputs, which we have denoted $D_{\alpha\alpha}(\langle X_i\rangle, \langle Y_i\rangle)$, is much slower than the average diffusion rate estimated by averaging all of the individual diffusion coefficients together, which we denoted $\langle D_{\alpha\alpha}(X_i, Y_i)\rangle$. In our experiments, we noted that the difference in $f(\alpha = 30°)$ after 30 days using these two different "averages" could be more than a factor of 10 at large pitch-angles (see Figure S1 in Supplemental Information), and around a factor of 3 at lower pitch-angles. These differences might depend sensitively on the location of diffusion "gaps" in pitch-angle, or on the size of the variance in the $D_{\alpha\alpha}(\alpha)$ distribution, or a combination of both. Our results strongly suggest that databases of many individual diffusion coefficients should be constructed from co-located and simultaneous measurements. Diffusion coefficient models could then be constructed using appropriate averages of these individual diffusion coefficients, or stochastic methods such as suggested here. Preliminary studies of these new methods of averaging suggest that they are more effective than previous methods (Ross et al., 2020).

Other evidence suggests it is important to understand the underlying distribution of diffusion coefficients. Idealized numerical experiments using a radial diffusion equation (Thompson et al., 2020) noted that the amount of diffusion depends upon the nature of the underlying distribution of diffusion coefficients. Those distributions with statistically heavier tails experienced greater diffusion, even when the distributions of diffusion coefficients had the same statistical average value.

The ensemble experiments are examples of probabilistic models that can yield rich information about the potential behaviour and uncertainty in the physical system. This uncertainty may exist due to a lack of knowledge, indicating that further parameterization of the diffusion coefficients is merited, perhaps using geomagnetic indices or other magnetospheric conditions. Or it may be true that there is inherent natural variability in the system that cannot be parameterized away.

5 Conclusions

We have presented the results from a series of idealized numerical experiments that highlight the response of the pitch-angle diffusion equation to temporally-varying diffusion coefficients that reproduce the full range of observation-specific wave-particle interactions observed over a four year period by NASA Van Allen probes. We present evidence to show that both the wave intensity, and number density observed in the same region of L^*, MLT and magnetic latitude over a period of around 30 days varies significantly, causing changes in $D_{\alpha\alpha}$ of orders of magnitude on timescales of less than 9 hours. We perform idealised numerical experiments of the resulting pitch-angle diffusion that could result from different methods of averaging the diffusion coefficient, as well as two ensemble experiments that deploy stochastic parameterization techniques. If the timescale of variability is very short (Δt = 2 minutes), then the ensemble result is very similar to the result using the average of many observation-specific coefficients. Where inputs to the diffusion coefficient are averaged prior to its calculation, then the amount of diffusion experienced is much less than in any other numerical experiment. Most interestingly, in the ensemble experiments where diffusion is varied on different timescales, the phase space density solution of the experiment with longer variability timescales (Δt = 6 hours) reaches lower values than in the experiment with faster timescales, even though the total time-integrated diffusion in each experiment is the same.

Both this paper and Thompson et al. (2020) highlight that the distribution and variability timescales of diffusion coefficients are important for the evolution of electron phase space density due to diffusion. In other words, key details of the microphysical wave-particle interaction are important for accurate modeling of the macroscale radiation belt system, and the evolution of phase-space density is not solely reliant on the average properties of the diffusion coefficients. Our preliminary results isolate pitch-angle scattering due to plasmaspheric hiss, but the concepts illustrated in this paper are likely to be important for all wave-particle interactions in the inner magnetosphere.

Acknowledgments

This research was supported by the Natural Environment Research Council (NERC) Highlight Topic Grant "Rad-Sat" NE/P017274/1 (CEJW), NE/P01738X/1 (NPM, SAG and RBM) and NE/P017185/1 (IJR). CEJW and SNB are further supported by STFC grant ST/R000921/1. HJA acknowledges Helmholtz-Gemeinshaft (HGF). RLT is supported by the Engineering and Physical Sciences Research Council (EPSRC) grant EP/L016613/1.

Diffusion coefficient data that are shown in Figure 1 can be found at http://dx.doi.org/10.17864/1947.212. Ensemble and averaged numerical experiment results can be found at http://dx.doi.org/10.5281/zenodo.4290006.

References

Allison, H. J., Horne, R. B., Glauert, S. A., & Del Zanna, G. (2019). On the importance of gradients in the low-energy electron phase space density for relativistic electron acceleration. *Journal of Geophysical Research: Space Physics*, *124*(4), 2628-2642. Retrieved from `https://agupubs.onlinelibrary.wiley.com/doi/abs/10.1029/2019JA026516` doi: 10.1029/2019JA026516

Berner, J., Achatz, U., Batt, L., Bengtsson, L., Cmara, A. d. l., Christensen, H. M., ... Yano, J.-I. (2017). Stochastic parameterization: Toward a new view of weather and climate models. *Bulletin of the American Meteorological Society*, *98*(3), 565-588. doi: 10.1175/BAMS-D-15-00268.1

Drozdov, A. Y., Shprits, Y. Y., Orlova, K. G., Kellerman, A. C., Subbotin, D. A., Baker, D. N., ... Reeves, G. D. (2015). Energetic, relativistic, and ultrarelativistic electrons: Comparison of long-term verb code simulations with van allen probes measurements. *Journal of Geophysical Research: Space Physics*,

120(5), 3574-3587. doi: 10.1002/2014JA020637

Glauert, S. A., & Horne, R. B. (2005). Calculation of pitch angle and energy diffusion coefficients with the padie code. *Journal of Geophysical Research: Space Physics*, *110*(A4). doi: 10.1029/2004JA010851

Glauert, S. A., Horne, R. B., & Meredith, N. P. (2014). Three-dimensional electron radiation belt simulations using the BAS Radiation Belt Model with new diffusion models for chorus, plasmaspheric hiss, and lightning-generated whistlers. *Journal of Geophysical Research: Space Physics*, *119*(1), 268-289. doi: 10.1002/2013JA019281

Glauert, S. A., Horne, R. B., & Meredith, N. P. (2018). A 30-year simulation of the outer electron radiation belt. *Space Weather*, *0*(0). doi: 10.1029/2018SW001981

Hartley, D. P., Kletzing, C. A., Santolk, O., Chen, L., & Horne, R. B. (2018). Statistical properties of plasmaspheric hiss from van allen probes observations. *Journal of Geophysical Research: Space Physics*, *123*(4), 2605-2619. doi: 10.1002/2017JA024593

Horne, R. B., Kersten, T., Glauert, S. A., Meredith, N. P., Boscher, D., Sicard-Piet, A., ... Li, W. (2013). A new diffusion matrix for whistler mode chorus waves. *Journal of Geophysical Research: Space Physics*, *118*(10), 6302-6318. doi: 10.1002/jgra.50594

Li, W., Ma, Q., Thorne, R. M., Bortnik, J., Kletzing, C. A., Kurth, W. S., ... Nishimura, Y. (2015). Statistical properties of plasmaspheric hiss derived from Van Allen Probes data and their effects on radiation belt electron dynamics. *Journal of Geophysical Research: Space Physics*, *120*(5), 3393-3405. doi: 10.1002/2015JA021048

Li, W., Ma, Q., Thorne, R. M., Bortnik, J., Zhang, X.-J., Li, J., ... Goldstein, J. (2016). Radiation belt electron acceleration during the 17 march 2015 geomagnetic storm: Observations and simulations. *Journal of Geophysical Research: Space Physics*, *121*(6), 5520-5536. Retrieved from `https://agupubs.onlinelibrary.wiley.com/doi/abs/10.1002/2016JA022400` doi: 10.1002/2016JA022400

Lyons, L. R., Thorne, R. M., & Kennel, C. F. (1972). Pitch-angle diffusion of radiation belt electrons within the plasmasphere. *Journal of Geophysical Research*, *77*(19), 3455-3474. doi: 10.1029/JA077i019p03455

Malaspina, D. M., Jaynes, A. N., Boul, C., Bortnik, J., Thaller, S. A., Ergun, R. E., ... Wygant, J. R. (2016). The distribution of plasmaspheric hiss wave power with respect to plasmapause location. *Geophysical Research Letters*, *43*(15), 7878-7886. doi: 10.1002/2016GL069982

Malaspina, D. M., Jaynes, A. N., Hospodarsky, G., Bortnik, J., Ergun, R. E., & Wygant, J. (2017). Statistical properties of low-frequency plasmaspheric hiss. *Journal of Geophysical Research: Space Physics*, *122*(8), 8340-8352. doi: 10.1002/2017JA024328

Malaspina, D. M., Ripoll, J.-F., Chu, X., Hospodarsky, G., & Wygant, J. (2018). Variation in plasmaspheric hiss wave power with plasma density. *Geophysical Research Letters*, *45*(18), 9417-9426. doi: 10.1029/2018GL078564

Meredith, N. P., Horne, R. B., Kersten, T., Li, W., Bortnik, J., Sicard, A., & Yearby, K. H. (2018). Global model of plasmaspheric hiss from multiple satellite observations. *Journal of Geophysical Research: Space Physics*, *123*(6), 4526-4541. doi: 10.1029/2018JA025226

Meredith, N. P., Horne, R. B., Shen, X.-C., Li, W., & Bortnik, J. (2020). Global model of whistler mode chorus in the near-equatorial region (—m—¡ 18). *Geophysical Research Letters*, *47*(11), e2020GL087311. doi: 10.1029/2020GL087311

Ripoll, J.-F., Claudepierre, S. G., Ukhorskiy, A. Y., Colpitts, C., Li, X., Fennell, J. F., & Crabtree, C. (2020). Particle dynamics in the earth's radiation belts:

Review of current research and open questions. *Journal of Geophysical Research: Space Physics*, *125*(5), e2019JA026735. doi: 10.1029/2019JA026735

Ripoll, J.-F., Loridan, V., Denton, M. H., Cunningham, G., Reeves, G., Santolk, O., ... Ukhorskiy, A. Y. (2019). Observations and fokker-planck simulations of the l-shell, energy, and pitch angle structure of earth's electron radiation belts during quiet times. *Journal of Geophysical Research: Space Physics*, *124*(2), 1125-1142. doi: 10.1029/2018JA026111

Ripoll, J.-F., Reeves, G. D., Cunningham, G. S., Loridan, V., Denton, M., Santolk, O., ... Ukhorskiy, A. Y. (2016). Reproducing the observed energy-dependent structure of Earth's electron radiation belts during storm recovery with an event-specific diffusion model. *Geophysical Research Letters*, *43*(11), 5616-5625. doi: 10.1002/2016GL068869

Ripoll, J.-F., Santolk, O., Reeves, G. D., Kurth, W. S., Denton, M. H., Loridan, V., ... Turner, D. L. (2017). Effects of whistler mode hiss waves in March 2013. *Journal of Geophysical Research: Space Physics*, *122*(7), 7433-7462. doi: 10.1002/2017JA024139

Ross, J. P. J., Glauert, S. A., Horne, R. B., Watt, C. E. J., Meredith, N. P., & Woodfield, E. E. (2020). A new approach to constructing models of electron diffusion by emic waves in the radiation belts. *Geophysical Research Letters*, *n/a*(n/a), e2020GL088976. doi: 10.1029/2020GL088976

Shprits, Y. Y., Subbotin, D., & Ni, B. (2009). Evolution of electron fluxes in the outer radiation belt computed with the VERB code. *Journal of Geophysical Research: Space Physics*, *114*(A11). doi: 10.1029/2008JA013784

Shprits, Y. Y., Subbotin, D. A., Meredith, N. P., & Elkington, S. R. (2008). Review of modeling of losses and sources of relativistic electrons in the outer radiation belt ii: Local acceleration and loss. *Journal of Atmospheric and Solar-Terrestrial Physics*, *70*(14), 1694 - 1713. (Dynamic Variability of Earth's Radiation Belts) doi: https://doi.org/10.1016/j.jastp.2008.06.014

Spasojevic, M., Shprits, Y. Y., & Orlova, K. (2015). Global empirical models of plasmaspheric hiss using Van Allen Probes. *Journal of Geophysical Research: Space Physics*, *120*(12), 10,370-10,383. doi: 10.1002/2015JA021803

Thompson, R. L., Watt, C. E. J., & Williams, P. D. (2020). Accounting for variability in ULF wave radial diffusion models. *Journal of Geophysical Research: Space Physics*, *125*(8), e2019JA027254. doi: 10.1029/2019JA027254

Tu, W., Cunningham, G. S., Chen, Y., Morley, S. K., Reeves, G. D., Blake, J. B., ... Spence, H. (2014). Event-specific chorus wave and electron seed population models in DREAM3D using the van allen probes. *Geophysical Research Letters*, *41*(5), 1359-1366. doi: 10.1002/2013GL058819

Wang, D., Shprits, Y. Y., Zhelavskaya, I. S., Agapitov, O. V., Drozdov, A. Y., & Aseev, N. A. (2019). Analytical chorus wave model derived from van allen probe observations. *Journal of Geophysical Research: Space Physics*, *124*(2), 1063-1084. doi: 10.1029/2018JA026183

Watt, C. E. J., Allison, H. J., Meredith, N. P., Thompson, R. L., Bentley, S. N., Rae, I. J., ... Horne, R. B. (2019). Variability of Quasilinear Diffusion Coefficients for Plasmaspheric Hiss. *Journal of Geophysical Research: Space Physics*, *124*(10), 9545-9551. doi: 10.1002/2018JA026401

Zhao, H., Friedel, R. H. W., Chen, Y., Reeves, G. D., Baker, D. N., Li, X., ... Spence, H. E. (2018). An empirical model of radiation belt electron pitch angle distributions based on van allen probes measurements. *Journal of Geophysical Research: Space Physics*, *123*(5), 3493-3511. doi: 10.1029/2018JA025277

Zhu, H., Shprits, Y. Y., Spasojevic, M., & Drozdov, A. Y. (2019). New hiss and chorus waves diffusion coefficient parameterizations from the van allen probes and their effect on long-term relativistic electron radiation-belt verb simulations. *Journal of Atmospheric and Solar-Terrestrial Physics*, *193*, 105090. Retrieved from `http://www.sciencedirect.com/science/article/pii/`

S1364682618304589 doi: https://doi.org/10.1016/j.jastp.2019.105090